

# Vanishing fine structure splittings in telecom wavelength quantum dots grown on (111)A surfaces by droplet epitaxy

Xiangming Liu,<sup>1</sup> Neul Ha,<sup>1,2</sup> Hideaki Nakajima,<sup>3</sup> Takaaki Mano,<sup>1</sup> Takashi Kuroda,<sup>1,2,\*</sup> Bernhard Urbaszek,<sup>4</sup> Hidekazu Kumano,<sup>3</sup> Ikuo Suemune,<sup>3</sup> Yoshiki Sakuma,<sup>1</sup> and Kazuaki Sakoda<sup>1</sup>

<sup>1</sup>*National Institute for Materials Science, 1-1 Namiki, Tsukuba 305-0044, Japan*

<sup>2</sup>*Graduate School of Engineering, Kyushu University, NIMS, Tsukuba 305-0044, Japan*

<sup>3</sup>*Research Institute for Electronic Science, Hokkaido University, Sapporo 001-0021, Japan*

<sup>4</sup>*Université de Toulouse, INSA-CNRS-UPS, LPCNO, 135 Av. Rangueil, 31077 Toulouse, France*

(Dated: March 1, 2022)

The emission cascade of a single quantum dot is a promising source of entangled photons. A prerequisite for this source is the use of a symmetric dot analogous to an atom in a vacuum, but the simultaneous achievement of structural symmetry and emission in a telecom band poses a challenge. Here we report the growth and characterization of highly symmetric InAs/InAlAs quantum dots self-assembled on  $C_{3v}$  symmetric InP(111)A. The broad emission spectra cover the O ( $\lambda \sim 1.3 \mu\text{m}$ ), C ( $\lambda \sim 1.55 \mu\text{m}$ ), and L ( $\lambda \sim 1.6 \mu\text{m}$ ) telecom bands. The distribution of the fine-structure splittings is considerably smaller than those reported in previous works on dots at similar wavelengths. The presence of dots with degenerate exciton lines is further confirmed by the optical orientation technique. Thus, our dot systems are expected to serve as efficient entangled photon emitters for long-distance fiber-based quantum key distribution.

Semiconductor quantum dots (QD) are expected to play a central role in quantum information networks. A noteworthy device based on dots is the solid-state single photon source, which ensures absolute security in quantum key distribution (QKD)<sup>1</sup>. Since QDs can confine charged carriers in nanometer-sized regions, recombination enables single photons to appear on demand, i.e., synchronously with a master clock shared in networks<sup>2</sup>. QKD over a 50 km commercial fiber has already been demonstrated with QD photon sources, which emitted at a wavelength of  $1.5 \mu\text{m}$ <sup>3</sup>. The transmission distance in that work was limited purely by the absorption loss of silicate fibers. Exceeding this fundamental limit requires the development of quantum link protocols, which exploit the nonlocality inherent in quantum theory. An efficient source of entangled photon pairs is a key element in the realization of such protocols, examples of which include quantum teleportation<sup>4</sup> and entanglement swapping<sup>5</sup>.

The generation of entangled photons with semiconductor QDs is directly linked to the singlet configuration of two excitons (X), which form a biexciton (XX). Eventually, two photons associated with the XX-X cascade show polarization correlations independent of the choice of measurement basis, yielding quantum entanglement in the polarization state. However, a common class of QDs exhibits considerable fine-structure splittings (FSS)<sup>6–10</sup>, which exclude entanglement in emitted photons<sup>11</sup>. Numerous attempts have been made to suppress FSS and recover the symmetry of QDs grown on conventional (001) oriented substrates<sup>12–19</sup>. However, from a practical point of view, the reproducible growth of symmetric dots with (at least) near-zero FSS is highly desirable.

A noteworthy strategy for achieving such high QD symmetry is the application of  $C_{3v}$  symmetric (111) surfaces to the growth substrate, as was predicted theoretically<sup>20</sup>. Although QD growth in the Stranski-Krastanov (SK) mode is prohibited along the [111] axis,

the use of patterned substrates<sup>21</sup> and droplet epitaxy<sup>22,23</sup> makes it possible to grow QDs on (111) substrates. Hence, a great reduction in FSS was observed in these QDs<sup>23,24</sup>, which led to the demonstration of entangled photon emission in pyramidal QDs on patterned (111)B substrates<sup>25</sup>, and the filtering-free violation of Bell's inequality for droplet epitaxial GaAs/AlGaAs dots on GaAs(111)A<sup>26</sup>. Note that all these studies dealt with visible wavelength photons. Material challenges have meant that the development of QD sources in telecom bands has achieved less progress. The simultaneous realization of small FSS and telecom-band emission is a great challenge.

In this work, we report on the growth and characterization of telecom-band InAs quantum dots on (111)A substrates. For this purpose, we focus on the use of droplet epitaxy, which is not strain driven, thereby enabling us to choose a variety of materials and surface orientations. Though most previous works on droplet epitaxy dealt with lattice-matched systems, the versatility of this technique makes it possible to create QDs on lattice-mismatched systems targeting telecom-band emission. The successful growth of InAs/InAlAs QDs on InP(111)A has recently been demonstrated<sup>27</sup>. Here we use newly created QDs with a lower surface density, which allows a systematic study of FSS and the symmetry characteristics of dots. The measured FSS reveals an average value of  $25 \mu\text{eV}$ , which is considerably smaller than those in previous studies on SK grown dots at similar wavelengths<sup>28–30</sup>. Moreover, the presence of QDs with nearly perfect exciton degeneracy is confirmed using the optical orientation technique. Thus our source is expected to serve as a promising candidate for highly efficient entangled photon sources, which do not require the use of serious temporal gating to improve the degree of quantum correlation<sup>31</sup>.

The sample investigated in this study was grown by

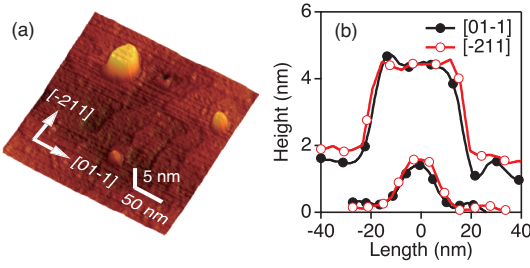


FIG. 1. (color online) (a) AFM image of the sample surface of InAs dots on  $\text{In}_{0.52}\text{Al}_{0.48}\text{As}/\text{InP}(111)\text{A}$ . (b) Cross sections along  $[01-1]$  and  $[-211]$  for a relatively large dot (top) and a small dot (bottom).

droplet epitaxy using a conventional molecular beam epitaxy apparatus<sup>32,33</sup>. After growing a 150-nm-thick  $\text{In}_{0.52}\text{Al}_{0.48}\text{As}$  barrier layer on an  $\text{InP}(111)\text{A}$  substrate at  $470^\circ\text{C}$ , we cooled the substrate to  $320^\circ\text{C}$  and supplied 0.4 monolayers of indium, which led to the formation of indium droplets. Next, we supplied an  $\text{As}_4$  flux of  $3 \times 10^{-5}$  Torr to crystallize the indium droplets into InAs dots at  $270^\circ\text{C}$ . The sample was then annealed at  $370^\circ\text{C}$  and capped with another  $\text{In}_{0.52}\text{Al}_{0.48}\text{As}$  barrier layer with a thickness of 75 nm.

For atomic force microscopy (AFM) analysis, an additional QD layer was grown on the top of the sample. Figure 1(a) shows a three-dimensional view of the surface, which reveals the presence of disk-like dots with  $3.0 (\pm 1.0)$  nm in height and  $38 (\pm 10)$  nm in diameter. The dot density is as low as  $3.2 \times 10^9 \text{ cm}^{-2}$ , which makes it possible to isolate single dots using conventional microphotoluminescence techniques. Figure 1(b) shows the AFM cross sections for two example QDs. Cross sections obtained along the orthogonal in-plane directions,  $[01-1]$  and  $[-211]$ , are almost identical, which supports the high lateral symmetry in the dot shape without any elongations. This symmetric characteristic is a consequence of QD growth on (111) substrates.

For the PL measurement we used a continuous wave laser emitting at a wavelength of 705 nm for excitation above the barrier band gap. The laser light was focused on the sample using a near-infrared microscope objective with a numerical aperture of 0.65. To reduce the spot size, a hemispherical solid immersion lens with a refractive index of two was positioned on the sample. Spontaneously emitted photons were collected with the same objective, and then fed into a 50-cm focal length polychromator equipped with an InGaAs array detector. The spectrometer had a resolution of  $55 \mu\text{eV}$  (0.08 nm) with a full width at half maximum (FWHM) at a wavelength of  $1.3 \mu\text{m}$ . The linearly polarized PL spectra were recorded as a function of the polarization angle. With a Gaussian fit to the emission lines, we were able to determine the spectral peak shift (and the absolute value of FSS) with a resolution as high as  $4 \mu\text{eV}$ . All the experiments were performed at 10 K.

Figure 2(a) shows the low-temperature PL spectrum

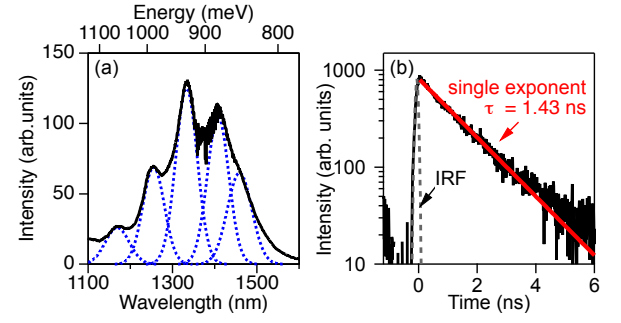


FIG. 2. (color online) (a) PL spectrum of the ensemble of dots. The blue broken lines show the results of multiple-peak fit with assuming Gaussian broadening for each peak. (c) Time-resolved PL signals after ps pulsed excitation. The gray broken line shows the instrumental response function (IRF). The red line shows a single exponential fit to the decay data with a lifetime of 1.43 ns.

of the dot ensembles. The PL spectrum spreads in a 1.1 to  $1.6 \mu\text{m}$  wavelength range, which covers the O ( $\lambda \sim 1310 \text{ nm}$ ), C ( $\lambda \sim 1550 \text{ nm}$ ), and L ( $\lambda \sim 1600 \text{ nm}$ ) telecom bands. The spectrum consists of several split peaks, among which high-yield emissions are centered at  $\sim 930 \text{ meV}$  (1333 nm) with an FWHM of 40 meV. The appearance of multiple peaks can be attributed to the different families of QDs with heights varying in monolayer steps<sup>23</sup>. The AFM analysis suggests that the QDs have a flat shape with a height that ranges from 2 to 6 monolayers, which is consistent with the observed spectral profile.

Figure 2(b) shows the PL decay signals of the dot ensembles at wavelengths around  $1.3 \mu\text{m}$  after pulsed excitation. For this measurement, we used a mode-locked Ti sapphire laser for excitation ( $\lambda \sim 785 \text{ nm}$ ) and a superconducting single photon detector (SSPD) for detection. The decay curve reveals a single exponent with a decay time of 1.43 ns, which agrees with the theoretical decay time of spontaneous emission on the assumption that the QDs have the same dipole moment as the bulk value. The similar decay times have been confirmed in telecom-wavelength QDs grown for different substrate orientations<sup>34</sup>. Thus, the observed PL decay is likely governed by intrinsic carrier recombination and free of any non-radiative process, as a consequence of the high crystalline quality of dots. The homogeneous linewidth, which gives the maximum limit of FSS for entangled photon emission, is thus  $\sim 0.5 \mu\text{eV}$  for our dots.

Figure 3(a) shows the typical PL spectrum of a single dot. Four emission lines are observed, and assigned, from the high-energy side, as  $X$ ,  $X^+$ ,  $XX$ , and  $X^-$ , where  $X^{+(-)}$  refers to positively (negatively) charged excitons. These assignments are based on the measurement of the excitation power dependence of the emission lines (Fig. 3(b)), where almost linear and quadratic behaviors were observed for  $X$  and  $XX$ , respectively. The assignment of  $X^+$  and  $X^-$  is further supported by an optical

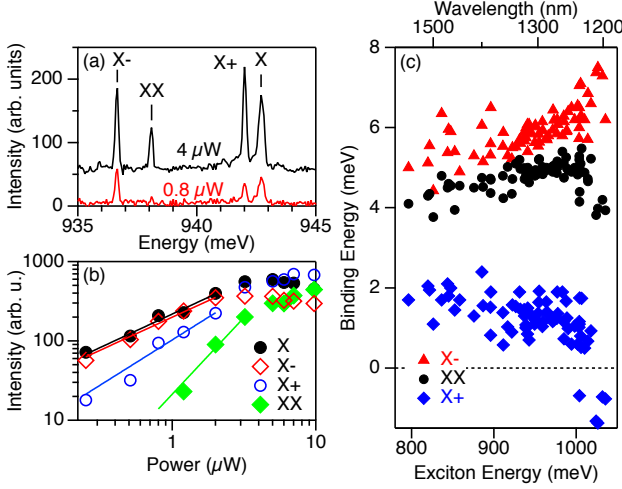


FIG. 3. (color online) (a) Typical PL spectra of a single QD with an excitation power of  $4 \mu\text{W}$  and  $0.8 \mu\text{W}$ . (b) PL intensity as a function of excitation power for each exciton complex. The solid lines show power laws,  $I \propto P^\alpha$ , where  $\alpha = 0.8, 0.8, 1.1$ , and  $1.8$  for  $X$ ,  $X^-$ ,  $X^+$ , and  $XX$ , respectively. (c) Evolution of the binding energy with the  $X$  energy for  $X^-$  (red triangles),  $XX$  (black circles), and  $X^+$  (blue diamonds).

orientation measurement, as described later.

Figure 3(c) shows the binding energy of each exciton complex as a function of  $X$  energy. Here the binding energy is defined as the energy difference between  $X$  and the exciton complex. It reveals that, with increasing  $X$  energy, the binding energy of  $X^-$  increases, that of  $X^+$  decreases, and that of  $XX$  has intermediate values. The mirror symmetric evolution of  $X^-$  and  $X^+$  is induced by the mean-field contribution to exciton charging<sup>35</sup>. Note that the spectral profile of exciton complexes is known to show a sensitive dependence on dot structure<sup>36</sup>. Therefore, the observation of a clear and less dispersive evolution in the binding energy suggests that the shape and other microscopic parameters of dots with a given size are almost identical. This is likely to be due to the kinetically limited formation of dots for droplet epitaxy. Consequently, dots on (111) substrates become rather symmetric as microscopic randomness is effectively suppressed.

Figures 4(a) and (b) show the evolution of the  $X$  peak energy when the linear polarization axis is rotated for two dots. The precise quantification of FSS is based on sinusoidal fitting to these evolutions, where the magnitude (absolute value) of FSS is defined as the amplitude of sine curves, and the polarization axis,  $\phi$ , is defined as the first maximum phase. Thus, the angle of  $\phi$  corresponds to the polarization axis of the high-energy  $X$  line among two split lines with orthogonal polarization. As shown by Figs. 4(a) and (b), both the FSS magnitude and polarization axis differ dot by dot.

The statistical results for FSS over 50 dots are sum-

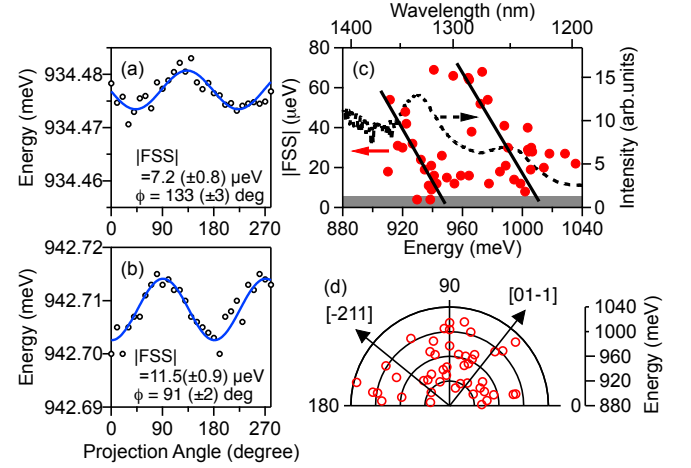


FIG. 4. (color online) (a, b) Energy shifts of the  $X$  line with rotating the axis of linear polarization for two dots. The blue lines are sinusoidal fits to the data. (c) Absolute value of FSS measured on single QDs (red circles). The broken line shows the ensemble PL spectrum. The solid lines are guides to the eye. (d) Polarization axis with respect to the emission energy. Two orthogonal in-plane axes  $[01-1]$  and  $[-211]$  are shown by arrows. The equivalent directions appear with every  $120^\circ$  rotation.

marized in Fig. 4(c), where the FSS magnitude is plotted as a function of  $X$  energy. The FSS ranges between 70 and  $3 \mu\text{eV}$ , where the minimum value is smaller than the error width of the present analysis ( $4 \mu\text{eV}$ , shown by the shaded region). The FSS average value is  $25 \mu\text{eV}$ , which is considerably smaller than those of SK grown QDs in the telecom band<sup>28–30</sup>. Note that two families of QDs with different monolayer heights are present in Fig. 4(c), as shown by the two peaks in the ensemble spectrum (broken line). Each family with a given height reveals a trend where the FSS decreases as the energy increases. This implies that high-energy QDs have a smaller in-plane size and higher lateral symmetry. The impact of the lateral-size reduction on FSS minimization was also confirmed in previous study on FSS control by high-temperature annealing<sup>12</sup>.

Figure 4(d) shows the direction of the polarization axis with respect to the  $X$  energy. They are randomly distributed, without showing significant correlations with the in-plane crystallographic axes. The absence of a preferential direction in the (111) plane suggests a high probability of finding QDs with negligible FSS over a broad spectral range.

The presence of dots with effectively zero FSS can be confirmed by measuring circularly polarized emission signals. In the presence of a finite FSS value, the polarization state of the emission light is expected to oscillate temporally between the left- and right-handed circular polarizations, where the oscillation period is determined by the inverse of the FSS. Therefore, in time-integrated experiments we cannot observe a high degree of circular

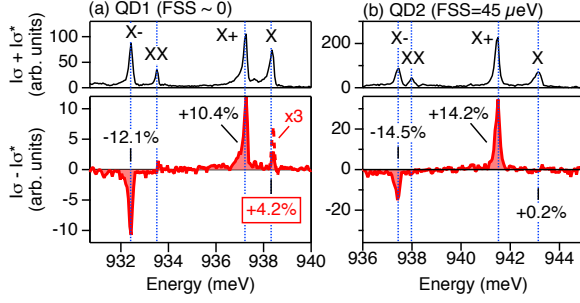


FIG. 5. (color online) Circularly-polarized emission signals with non-resonant circularly-polarized pump at a wavelength of 705 nm for (a) QD without a detectable FSS, and (b) QD with a finite value of FSS. Upper panels show unpolarized spectra. Lower panels show differential spectra between circular signals and cross-circular signals. The degree of circular polarization,  $(I_\sigma - I_{\sigma^*}) / (I_\sigma + I_{\sigma^*})$ , of each emission line is also shown.

polarization. By contrast, in the absence of FSS, circular polarization remains in time-integrated signals after circular injection. Thus, the observation of circular polarization provides a sufficient condition for exciton degeneracy. The measurement principle is analogous to the well-known Hanle measurement, and was used to monitor FSS cancellation by an electric field<sup>37</sup>. To avoid the effect of dynamic nuclear polarization<sup>38</sup>, we set the excitation power at a sufficiently low level, where the average exciton population in the dot was  $\sim 0.5$ .

Figures 5(a) and (b) show optical orientation results for a selected dot without a detectable FSS ( $< 4 \mu\text{eV}$ , QD1) and for a dot with a significant FSS ( $\sim 45 \mu\text{eV}$ , QD2), respectively. The upper panels show unpolarized spectra,  $I_\sigma + I_{\sigma^*}$ , where  $I_\sigma$  ( $I_{\sigma^*}$ ) is the emission intensity with co-circular (cross-circular) polarization with respect to the excitation light. The lower panels show the differential spectra,  $I_\sigma - I_{\sigma^*}$ , where a pronounced positive peak appears for the X line of QD1, but disappears for that of QD2. The positive degree of polarization for the X line of QD1 (+4.2%) is evidence of the degenerate exciton states. By contrast, the XX line does not exhibit a significant polarization in both QD1 and QD2, because the transition from XX comprises two routes with orthogonal polarizations. The other spectral lines follow well-known dynamics:  $X^+$  shows a positive degree of polarization, which is due to spin-polarized electron injection.  $X^-$  shows a negative degree of polarization, which is accompanied by the spin-flip relaxation of electrons<sup>39,40</sup>.

Note that only a few dots exhibit circular polarization for the X line. A rough estimation of the probability of finding dots with a circularly polarized X line is  $\sim 2\%$ , which agrees with the ratio of the natural width of our dots ( $0.5 \mu\text{eV}$ ) divided by the distribution of FSS ( $25 \mu\text{eV}$ ). This small probability reflects the relatively long emission lifetime of telecom-wavelength dots as compared with that of visible-wavelength dots. Optical orientation therefore serves as an efficient way to select dots

suitable for entangled photon generation. Although it is not essentially difficult to find dots with effectively zero FSS, a combination of external tuning protocols is also beneficial, where only a small tuning range is required to reach the optimum conditions in our dots.

Recent theoretical attempts based on first-principle calculations suggest the influence of atomic-scale symmetry breaking on the emergence of FSS<sup>41</sup>. Such microscopic asymmetry comes from interfacial randomness at hetero surfaces and compositional fluctuations inside and outside dots. It is noteworthy that the distribution of the measured FSS in our dots is smaller than that theoretically predicted for telecom dots on (100) surfaces, in which a perfectly symmetric shape was assumed<sup>42</sup>. This implies that the [111] grown dots are more stable against microscopic disorder than the [100] grown dots.

We attribute the further reduction of FSS in the [111] grown dots compared with that of conventional [100] grown dots to two mechanisms. First, owing to the high surface stability of the (111) plane, the dots have atomically flat surfaces, which were demonstrated by transmission electron microscopy analysis<sup>27</sup>. The smooth and abrupt interface also leads to the observation of distinct spectral multiplets in ensemble spectra (Fig. 2(a)). Thus, we expect the effect of interfacial randomness on FSS to be greatly suppressed compared with SK-grown (100) dots. Second, in zinc-blend compound semiconductors, the piezoelectric field direction is along the [111] polar axis, which coincides with the vertical growth direction in our system. Thus, a strain field does not induce any great reduction in lateral symmetry. The (111) surface is thus an ideal substrate for the growth of symmetric dots, where both geometrical (shape) symmetry and atomic-scale symmetry are well conserved.

In summary, we have presented measurements of minimized FSS in telecom-wavelength InAs QDs on an InP(111)A substrate prepared by droplet epitaxy. Polarization-resolved PL measurements were performed to examine the FSS distribution. Resolution-limited splittings (smaller than  $4 \mu\text{eV}$ ) were confirmed. The random distribution of the polarization axis made it possible to find symmetric dots over a wide spectral range. Thus our InAs/InAlAs dots on (111) substrates can play a crucial role in quantum information processing as an efficient entangled photon source that can work in telecom fiber networks.

- \* kuroda.takashi@nims.go.jp
- <sup>1</sup> A. Zeilinger, “Experiment and the foundations of quantum physics,” *Rev. Mod. Phys.* **71**, S288–S297 (1999); N. Gisin, G. Ribordy, W. Tittel, and H. Zbinden, “Quantum cryptography,” *Rev. Mod. Phys.* **74**, 145–195 (2002).
  - <sup>2</sup> O. Benson, C. Santori, M. Pelton, and Y. Yamamoto, “Regulated and entangled photons from a single quantum dot,” *Phys. Rev. Lett.* **84**, 2513–2516 (2000).
  - <sup>3</sup> K. Takemoto, Y. Nambu, T. Miyazawa, K. Wakui, S. Hirose, T. Usuki, M. Takatsu, N. Yokoyama, K. Yoshino, A. Tomita, S. Yorozu, Y. Sakuma, and Y. Arakawa, “Transmission experiment of quantum keys over 50 km using high-performance quantum-dot single-photon source at 1.5  $\mu\text{m}$  wavelength,” *Appl. Phys. Express* **3**, 092802 (2010).
  - <sup>4</sup> C. H. Bennett, G. Brassard, C. Crépeau, R. Jozsa, A. Peres, and W. K. Wootters, “Teleporting an unknown quantum state via dual classical and Einstein-Podolsky-Rosen channels,” *Phys. Rev. Lett.* **70**, 1895–1899 (1993).
  - <sup>5</sup> M. Żukowski, A. Zeilinger, M. A. Horne, and A. K. Ekert, ““Event-ready-detectors” Bell experiment via entanglement swapping,” *Phys. Rev. Lett.* **71**, 4287–4290 (1993); S. Bose, V. Vedral, and P. L. Knight, “Multi-particle generalization of entanglement swapping,” *Phys. Rev. A* **57**, 822–829 (1998); J.-W. Pan, D. Bouwmeester, H. Weinfurter, and A. Zeilinger, “Experimental entanglement swapping: Entangling photons that never interacted,” *Phys. Rev. Lett.* **80**, 3891–3894 (1998).
  - <sup>6</sup> D. Gammon, E. S. Snow, B. V. Shanabrook, D. S. Katzer, and D. Park, “Fine structure splitting in the optical spectra of single GaAs quantum dots,” *Phys. Rev. Lett.* **76**, 3005–3008 (1996).
  - <sup>7</sup> M. Bayer, A. Kuther, A. Forchel, A. Gorbunov, V. B. Timofeev, F. Schäfer, J. P. Reithmaier, T. L. Reinecke, and S. N. Walck, “Electron and hole  $g$  factors and exchange interaction from studies of the exciton fine structure in  $\text{In}_{0.60}\text{Ga}_{0.40}\text{As}$  quantum dots,” *Phys. Rev. Lett.* **82**, 1748–1751 (1999).
  - <sup>8</sup> V. D. Kulakovskii, G. Bacher, R. Weigand, T. Kummell, A. Forchel, E. Borovitskaya, K. Leonardi, and D. Hommel, “Fine structure of biexciton emission in symmetric and asymmetric CdSe/ZnSe single quantum dots,” *Phys. Rev. Lett.* **82**, 1780–1783 (1999).
  - <sup>9</sup> R. Seguin, A. Schliwa, S. Rodt, K. Pötschke, U. W. Pohl, and D. Bimberg, “Size-dependent fine-structure splitting in self-organized InAs/GaAs quantum dots,” *Phys. Phys. Lett.* **95**, 257402 (2005).
  - <sup>10</sup> M. Abbarchi, C. A. Mastrandrea, T. Kuroda, T. Mano, K. Sakoda, N. Koguchi, S. Sanguinetti, A. Vinattieri, and M. Gurioli, “Exciton fine structure in strain-free GaAs/ $\text{Al}_{0.3}\text{Ga}_{0.7}\text{As}$  quantum dots: Extrinsic effects,” *Phys. Rev. B* **78**, 125321 (2008).
  - <sup>11</sup> C. Santori, D. Fattal, M. Pelton, G. S. Solomon, and Y. Yamamoto, “Polarization-correlated photon pairs from a single quantum dot,” *Phys. Rev. B* **66**, 045308 (2002).
  - <sup>12</sup> W. Langbein, P. Borri, U. Woggon, V. Stavarache, D. Reuter, and A. D. Wieck, “Control of fine-structure splitting and biexciton binding in  $\text{In}_x\text{Ga}_{1-x}\text{As}$  quantum dots by annealing,” *Phys. Rev. B* **69**, 161301(R) (2004); R. J. Young, R. M. Stevenson, A. J. Shields, P. Atkinson, K. Cooper, D. A. Ritchie, K. M. Groom, A. I. Tartakovskii, and M. S. Skolnick, “Inversion of exciton level splitting in quantum dots,” *Phys. Rev. B* **72**, 113305 (2005).
  - <sup>13</sup> N. Akopian, N. H. Lindner, E. Poem, Y. Berlatzky, J. Avron, D. Gershoni, B. D. Gerardot, and P. M. Petroff, “Entangled photon pairs from semiconductor quantum dots,” *Phys. Rev. Lett.* **96**, 130501 (2006).
  - <sup>14</sup> R. M. Stevenson, R. J. Young, P. Atkinson, K. Cooper, D. A. Ritchie, and A. J. Shields, “A semiconductor source of triggered entangled photon pairs,” *Nature* **439**, 178–182 (2006); M. A. Pooley, A. J. Bennett, R. M. Stevenson, A. J. Shields, I. Farrer, and D. A. Ritchie, “Energy-tunable quantum dot with minimal fine structure created by using simultaneous electric and magnetic fields,” *Phys. Rev. Applied* **1**, 024002 (2014).
  - <sup>15</sup> S. Seidl, M. Kroner, A. Högele, K. Karrai, R. J. Warburton, A. Badolato, and P. M. Petroff, “Effect of uniaxial stress on excitons in a self-assembled quantum dot,” *Appl. Phys. Lett.* **88**, 203113 (2006); B. D. Gerardot, S. Seidl, P. A. Dalgarno, R. J. Warburton, D. Granados, J. M. Garcia, K. Kowalik, O. Krebs, K. Karrai, A. Badolato, and P. M. Petroff, “Manipulating exciton fine structure in quantum dots with a lateral electric field,” *Appl. Phys. Lett.* **90**, 041101 (2007).
  - <sup>16</sup> A. Muller, W. Fang, J. Lawall, and G. S. Solomon, “Creating polarization-entangled photon pairs from a semiconductor quantum dot using the optical Stark effect,” *Phys. Rev. Lett.* **103**, 217402 (2009).
  - <sup>17</sup> A. Dousse, J. Suffczynski, A. Beveratos, O. Krebs, A. Lemaître, I. Sagnes, J. Bloch, P. Voisin, and P. Senellart, “Ultrabright source of entangled photon pairs,” *Nature* **466**, 217–220 (2010).
  - <sup>18</sup> M. Ghali, K. Ohtani, Y. Ohno, and H. Ohno, “Generation and control of polarization-entangled photons from GaAs island quantum dots by an electric field,” *Nat. Commun.* **3**:661 (2012), 10.1038/ncomms1657; M. A. Pooley, A. J. Bennett, I. Farrer, D. A. Ritchie, and A. J. Shields, “Engineering quantum dots for electrical control of the fine structure splitting,” *Appl. Phys. Lett.* **103**, 031105 (2013).
  - <sup>19</sup> R. Trotta, E. Zallo, C. Ortix, P. Atkinson, J. D. Plumhof, J. van den Brink, A. Rastelli, and O. G. Schmidt, “Universal recovery of the energy-level degeneracy of bright excitons in InGaAs quantum dots without a structure symmetry,” *Phys. Rev. Lett.* **109**, 147401 (2012); R. Trotta, J. S. Wildmann, E. Zallo, O. G. Schmidt, and A. Rastelli, “Highly entangled photons from hybrid piezoelectric-semiconductor quantum dot devices,” arXiv:1403.0225.
  - <sup>20</sup> R. Singh and G. Bester, “Nanowire quantum dots as an ideal source of entangled photon pairs,” *Phys. Rev. Lett.* **103**, 063601 (2009); A. Schliwa, M. Winkelnkemper, A. Lochmann, E. Stock, and D. Bimberg, “In(Ga)As/GaAs quantum dots grown on a (111) surface as ideal sources of entangled photon pairs,” *Phys. Rev. B* **80**, 161307 (2009).
  - <sup>21</sup> Y. Sugiyama, Y. Sakuma, S. Muto, and N. Yokoyama, “Novel InGaAs/GaAs quantum dot structures formed in tetrahedral-shaped recesses on (111)B GaAs substrate using metalorganic vapor phase epitaxy,” *Appl. Phys. Lett.* **67**, 256–258 (1995); A. Hartmann, Y. Ducommun, L. Loubies, K. Leifer, and E. Kapon, “Structure and photoluminescence of single AlGaAs/GaAs quantum dots grown in inverted tetrahedral pyramids,” *Appl. Phys. Lett.* **73**, 2322–2324 (1998); L. O. Mereni, V. Dimastrodonato, R. J.



- Young, and E. Pelucchi, "A site-controlled quantum dot system offering both high uniformity and spectral purity," *Appl. Phys. Lett.* **94**, 223121 (2009).
- <sup>22</sup> E. Stock, T. Warming, I. Ostapenko, S. Rodt, A. Schliwa, J. A. Töfflinger, A. Lochmann, A. I. Toropov, S. A. Moshchenko, D. V. Dmitriev, V. A. Haisler, and D. Bimberg, "Single-photon emission from InGaAs quantum dots grown on (111) GaAs," *Appl. Phys. Lett.* **96**, 093112 (2010).
- <sup>23</sup> T. Mano, M. Abbarchi, T. Kuroda, B. McSkimming, A. Ohtake, K. Mitsuishi, and K. Sakoda, "Self-assembly of symmetric GaAs quantum dots on (111)A substrates: Suppression of fine-structure splitting," *Appl. Phys. Express* **3**, 065203 (2010); M. Jo, T. Mano, M. Abbarchi, T. Kuroda, Y. Sakuma, and K. Sakoda, "Self-limiting growth of hexagonal and triangular quantum dots on (111)A," *Cryst. Growth Des.* **12**, 1411–1415 (2012).
- <sup>24</sup> K. F. Karlsson, M. A. Dupertuis, D. Y. Oberli, E. Pelucchi, A. Rudra, P. O. Holtz, and E. Kapon, "Fine structure of exciton complexes in high-symmetry quantum dots: Effects of symmetry breaking and symmetry elevation," *Phys. Rev. B* **81**, 161307 (2010); L. O. Mereni, O. Marquardt, G. Juska, V. Dimastrodonato, E. P. O'Reilly, and E. Pelucchi, "Fine-structure splitting in large-pitch pyramidal quantum dots," *Phys. Rev. B* **85**, 155453 (2012).
- <sup>25</sup> G. Juska, V. Dimastrodonato, L. O. Mereni, A. Gocalinska, and E. Pelucchi, "Towards quantum-dot arrays of entangled photon emitters," *Nature Photon.* **7**, 527 (2013).
- <sup>26</sup> T. Kuroda, T. Mano, N. Ha, H. Nakajima, H. Kumano, B. Urbaszek, M. Jo, M. Abbarchi, Y. Sakuma, K. Sakoda, I. Suemune, X. Marie, and T. Amand, "Symmetric quantum dots as efficient sources of highly entangled photons: Violation of Bell's inequality without spectral and temporal filtering," *Phys. Phys. B* **88**, 041306(R) (2013).
- <sup>27</sup> N. Ha, X. Liu, T. Mano, T. Kuroda, K. Mitsuishi, A. Castellano, S. Sanguinetti, T. Noda, Y. Sakuma, and K. Sakoda, "Droplet epitaxial growth of highly symmetric quantum dots emitting at telecommunication wavelengths on InP(111)A," *Appl. Phys. Lett.* **104**, 143106 (2014).
- <sup>28</sup> N. I. Cade, H. Gotoh, H. Kamada, H. Nakano, and H. Okamoto, "Fine structure and magneto-optics of exciton, trion, and charged biexciton states in single InAs quantum dots emitting at 1.3  $\mu\text{m}$ ," *Phys. Rev. B* **73**, 115322 (2006).
- <sup>29</sup> N. Chauvin, B. Salem, G. Bremond, G. Guillot, C. Bruchevallier, and M. Gendry, "Size and shape effects on excitons and biexcitons in single InAs/InP quantum dots," *J. Appl. Phys.* **100**, 073702 (2006).
- <sup>30</sup> L. Sapienza, R. N. E. Malein, C. E. Kuklewicz, P. E. Kremer, K. Srinivasan, A. Griffiths, E. Clarke, M. Gong, R. J. Warburton, and B. D. Gerardot, "Exciton fine-structure splitting of telecom-wavelength single quantum dots: Statistics and external strain tuning," *Phys. Rev. B* **88**, 155330 (2013).
- <sup>31</sup> M. B. Ward, M. C. Dean, R. M. Stevenson, A. J. Bennett, D. J. P. Ellis, K. Cooper, I. Farrer, C. A. Nicoll, D. A. Ritchie, and A. J. Shields, "Coherent dynamics of a telecom-wavelength entangled photon source," *Nat. Commun.* **5**:3316 (2014), 10.1038/ncomms4316.
- <sup>32</sup> N. Koguchi, S. Takahashi, and T. Chikyow, "New MBE growth method for InSb quantum well boxes," *J. Cryst. Growth* **111**, 688–692 (1991); T. Mano, M. Abbarchi, T. Kuroda, C. A. Mastrandrea, A. Vinattieri, S. Sanguinetti, K. Sakoda, and M. Gurioli, "Ultra-narrow emission from single GaAs self-assembled quantum dots grown by droplet epitaxy," *Nanotechnology* **20**, 395601 (2009).
- <sup>33</sup> G. Sallen, B. Urbaszek, M. M. Glazov, E. L. Ivchenko, T. Kuroda, T. Mano, S. Kunz, M. Abbarchi, K. Sakoda, D. Lagarde, A. Balocchi, X. Marie, and T. Amand, "Dark-bright mixing of interband transitions in symmetric semiconductor quantum dots," *Phys. Rev. Lett.* **107**, 166604 (2011); G. Sallen, S. Kunz, T. Amand, L. Bouet, T. Kuroda, T. Mano, D. Paget, O. Krebs, X. Marie, K. Sakoda, and B. Urbaszek, "Nuclear magnetization in gallium arsenide quantum dots at zero magnetic field," *Nat. Commun.* **5**:3268 (2014), 10.1038/ncomms4268.
- <sup>34</sup> C. Zinoni, B. Alloing, C. Monat, V. Zwiller, L. H. Li, A. Fiore, L. Lugi, A. Gerardino, H. de Riedmatten, H. Zbinden, and N. Gisin, "Time-resolved and antibunching experiments on single quantum dots at 1300nm," *Appl. Phys. Lett.* **88**, 131102 (2006); K. Takemoto, M. Takatsu, S. Hirose, N. Yokoyama, Y. Sakuma, T. Usuki, T. Miyazawa, and Y. Arakawa, "An optical horn structure for single-photon source using quantum dots at telecommunication wavelength," *J. Appl. Phys.* **101**, 081720 (2007); P. Miska, J. Even, O. Dehaese, and X. Marie, "Carrier relaxation dynamics in InAs/InP quantum dots," *Appl. Phys. Lett.* **92**, 191103 (2008).
- <sup>35</sup> M. Abbarchi, T. Kuroda, T. Mano, K. Sakoda, C. A. Mastrandrea, A. Vinattieri, M. Gurioli, and T. Tsuchiya, "Energy renormalization of exciton complexes in GaAs quantum dots," *Phys. Rev. B* **82**, 201301(R) (2010).
- <sup>36</sup> V. Mlinar and A. Zunger, "Spectral barcoding of quantum dots: Deciphering structural motifs from the excitonic spectra," *Phys. Rev. B* **80**, 035328 (2009).
- <sup>37</sup> K. Kowalik, O. Krebs, A. Lemaître, B. Eble, A. Kudelski, P. Voisin, S. Seidl, and J. A. Gaj, "Monitoring electrically driven cancellation of exciton fine structure in a semiconductor quantum dot by optical orientation," *Appl. Phys. Lett.* **91**, 183104 (2007).
- <sup>38</sup> T. Belhadj, C.-M. Simon, T. Amand, P. Renucci, B. Chatel, O. Krebs, A. Lemaître, P. Voisin, X. Marie, and B. Urbaszek, "Controlling the polarization eigenstate of a quantum dot exciton with light," *Phys. Rev. Lett.* **103**, 086601 (2009).
- <sup>39</sup> S. Cortez, O. Krebs, S. Laurent, M. Senes, X. Marie, P. Voisin, R. Ferreira, G. Bastard, J.-M. Gérard, and T. Amand, "Optically driven spin memory in n-doped InAs-GaAs quantum dots," *Phys. Rev. Lett.* **89**, 207401 (2002).
- <sup>40</sup> A. S. Bracker, E. A. Stinaff, D. Gammon, M. E. Ware, J. G. Tischler, A. Shabaev, A. L. Efros, D. Park, D. Gershoni, V. L. Korenev, and I. A. Merkulov, "Optical pumping of the electronic and nuclear spin of single charge-tunable quantum dots," *Phys. Rev. Lett.* **94**, 047402 (2005).
- <sup>41</sup> G. Bester, S. Nair, and A. Zunger, "Pseudopotential calculation of the excitonic fine structure of million-atom self-assembled  $\text{In}_{1-x}\text{Ga}_x\text{As}$ /GaAs quantum dots," *Phys. Rev. B* **67**, 161306 (2003); L. He, M. Gong, C.-F. Li, G.-C. Guo, and A. Zunger, "Highly reduced fine-structure splitting in InAs/InP quantum dots offering an efficient on-demand entangled 1.55- $\mu\text{m}$  photon emitter," *Phys. Rev. Lett.* **101**, 157405 (2008).
- <sup>42</sup> E. Goldmann, S. Barthel, M. Florian, K. Schuh, and F. Jahnke, "Excitonic fine-structure splitting in telecom-wavelength InAs/GaAs quantum dots: Statistical distribution and height-dependence," *Appl. Phys. Lett.* **103**, 242102 (2013).